SCIENTIFIC REPORTS

The hemocompatibility of oxidized diamond nanocrystals for biomedical applications

Hung-Cheng Li[1]*, Feng-Jen Hsieh[1]*, Ching-Pin Chen[2,3], Ming-Yao Chang[2,3], Patrick C. H. Hsieh[2,3,4], Chia-Chun Chen[5], Shain-Un Hung[6], Che-Chih Wu[6] & Huan-Cheng Chang[1]

[1]Institute of Atomic and Molecular Sciences, Academia Sinica, Taipei 106, Taiwan, [2]Institute of Clinical Medicine, National Cheng Kung University & Hospital, Tainan 704, Taiwan, [3]Department of Biomedical Engineering, National Cheng Kung University & Hospital, Tainan 704, Taiwan, [4]Institute of Biomedical Sciences, Academia Sinica, Taipei 115, Taiwan, [5]Department of Chemistry, National Taiwan Normal University, Taipei 116, Taiwan, [6]Department of Applied Chemistry, National Chi Nan University, Puli, Nantou 545, Taiwan.

Low-dimensional carbon-based nanomaterials have recently received enormous attention for biomedical applications. However, increasing evidence indicates that they are cytotoxic and can cause inflammatory responses in the body. Here, we show that monocrystalline nanodiamonds (NDs) synthesized by high-pressure-high-temperature (HPHT) methods and purified by air oxidation and strong oxidative acid treatments have excellent hemocompatibility with negligible hemolytic and thrombogenic activities. Cell viability assays with human primary endothelial cells suggested that the oxidized HPHT-NDs (dimensions of 35–500 nm) are non-cytotoxic. No significant elevation of the inflammatory cytokine levels of IL-1β and IL-6 was detected in mice after intravenous injection of the nanocrystals *in vivo*. Using a hindlimb-ischemia mouse model, we demonstrated that 35-nm NDs after covalent conjugation with polyarginine are useful as a drug delivery vehicle of heparin for prolonged anticoagulation treatment. The present study lays a solid foundation for further therapeutic applications of NDs in biomedicine.

N anocarbon particles are promising nanomaterials for biomedical and bioengineering applications[1,2]. Members of the nanocarbon family include fullerenes, carbon nanotubes, graphenes, and nanodiamonds. Although carbon-based nanoparticles are generally considered to be biocompatible, properties such as electron configuration, particle size, surface charge, surface modification, and morphology are also determinants of the biocompatibility[3–6]. One-dimensional carbon nanotubes (CNTs) and two-dimensional graphene sheets (GSs) are excellent examples in this regard[6]. The latter in particular has recently attracted considerable attention and been extensively investigated for their toxicity and potential biomedical applications[7]. However, similar to the CNT cases, results of the biocompatibility and toxicity studies conducted for both pristine and functionalized GSs are controversial[7–15]. More rigorous research is needed to resolve the controversy.

In comparison to CNTs and GSs, nanodiamonds (NDs) are considerably less toxic[16,17]. This is attributed to the material's unique physicochemical properties, including sp[3] electron configuration, extreme chemical inertness, low aspect ratios, and easy purification by strong acid treatment to remove metal and other residual contaminants[18]. Despite that a large number of experiments on the cytotoxicity of diamond and other carbon nanoparticles have been performed[4], most of these previous studies used immortal cell lines *in vitro*. There is a need to evaluate the compatibility of the nanoparticles with normal cells, such as red blood cells (RBCs). Understanding the blood compatibility (or hemocompatibility) is vital in the context that the majority of the nanoparticles applied *in vivo* are intended to be administered through the bloodstream[19]. How they affect the functionalities of blood cells and other components is of primary concern when using NDs as nanoparticle-based therapeutic agents in animals[20,21].

Among the four different types of carbon nanoparticles, C$_{60}$ is known to cause hemolysis through oxidative stress-mediated damage of the erythrocyte membrane[22]. CNTs (both single-walled and multi-walled), on the other hand, can induce platelet aggregation and vascular thrombosis[23–25]. The thrombogenic potentials, however, can be substantially moderated through covalent functionalization with carboxyl or amino groups and surfactant coatings[24]. Similarly for GSs and graphene oxides (GOs), distinct dose-dependent hemolytic activities have been observed and covering of the nanosheets with biopolymers such as chitosan can effectively eliminate the toxicity[10].

As to nanoscale diamond, it has been reported that NDs synthesized by detonation (denoted as DNDs) can cause destruction of both white and red blood cells *in vitro*[26], and carboxylated DNDs can activate blood platelets and induce thromboembolism[27]. However, it is known that DND is structurally imperfect and its surface is covered with multilayer graphitic carbon shells. Moreover, the shell thickness as well as the purity and surface chemistry of the nanomaterials vary substantially with suppliers, making results obtained by different research groups difficult to compare. To avoid the complications, we chose to use nano-sized diamond crystallites synthesized by high-pressure-high-temperature (HPHT) methods as the samples[28]. These HPHT-NDs can be thoroughly purified by air oxidation and strong oxidative acid treatments, allowing elimination of all possible contaminants and graphitic surface layers prior to analysis.

The aims of this work are to study systematically the hemocompatibility of HPHT-NDs using hemolysis and thrombosis assays and to show the usefulness of polyarginine-coated ND particles as heparin carriers for prolonged anticoagulation treatment. Heparin (HP) is a biopolymer consisting of a variably sulfated repeating disaccharide unit comprising a D-glucosamine (GlcN) and an 1,4-linked uronic acid e.g. D-glucuronic acid (GlcA) or L-iduronic acid (IdoA)[29]. The polymer is highly sulfated, containing up to 3 sulfate groups in each disaccharide unit. Native HP typically has a molecular weight (MW) ranging from 3 kDa to 30 kDa and is commercially available as heparin sodium salts usually made from the extracts of pig intestines. The substance has been routinely used in medicine as an anticoagulant, which prevents fibrin formation by activating antithrombin III (AT-III), a protein that blocks thrombin from clotting blood. It is particularly useful for the treatment of deep vein thrombosis and other venous thrombosis diseases. However, a drawback of the treatment is that systemic (long-term) administration of HP may result in serious side effects such as thrombocytopenia and prolonged bleeding[30].

An often applied strategy to overcome the drawback of HP is to covalently immobilize HP on stationary surface, such as that of thermosensitive hydrogel[31], silica xerogels[32], and nanomaterials including CNTs[33]. Very recently, Tang *et al.*[34] employed HP-conjugated carbon nanocapsules (dimensions of 20–50 nm) to treat acute thromboembolism in mice via intravenous (i.v.) injection. Their results showed that the nanocapsules conjugated with HP have the ability to extend the blood flow to a longer time period than free HP in treating thrombosis induced with FeCl$_3$. Although carbon nanocapsules are less toxic than CNTs because of having lower aspect ratios and less edge defects[35], the particles can induce blood coagulation, a behavior resembling that of CNTs[34]. It raises concerns about using this sp^2-carbon-based material for biomedical applications. In this work, we demonstrate that both oxidized and HP-conjugated NDs are free of the undesirable effects. They are biologically safe and potentially useful for the treatment of blood-related diseases.

Results

Characterization of oxidized and HP-conjugated NDs. A critical step in diagnostic and therapeutic applications of nanoparticles is to conjugate biologically active agents to the particles' surfaces. In this context, NDs are advantageous over other non-carbon-based nanomaterials in terms of the easiness of surface modification and conjugation with biomolecules. Diamond surfaces, for example, can be readily functionalized with a variety of oxygen-containing groups after oxidation in air or purification in strong oxidative acids[36]. Approximately 10% of the surface carbon atoms on oxidative-acid-treated HPHT-NDs are in form of –COOH[37]. This amount of carboxyl groups is sufficient for ensuing conjugation with polylysine (PL)[36], polyarginine (PA)[38,39], or other polycationic polymers[40] by forming amide bonds through carbodiimide chemistry as illustrated in the experimental section.

Figure 1a presents a typical transmission electron microscopy (TEM) image of the ND sample used in this work. The NDs (dimensions of ~ 35 nm) are monocrystalline (**Figure 1b**), showing two characteristic peaks at $2\theta = 43.6°$ and $75.0°$ of diamond in powder X-ray diffraction spectra (**Figure 1c**). Dynamic light scattering indicated a hydrodynamic size (d_h) of 38 nm, along with a zeta potential (ξ) of −34 mV, for the nanocrystals dispersed in distilled deionized water (DDW). The size subsequently increased to $d_h = 77$ nm and the potential's polarity and magnitude changed to $\xi = +52$ mV when the NDs were covalently conjugated with PA. They further changed to $d_h = 91$ nm and $\xi = −43$ mV upon physical adsorption of HP onto the PA-ND surfaces (**Table 1** and **Figure 1d**). The amount of HP attached to the nanocrystals is ~ 5% (w/w) at saturation, as estimated from the loss of the total weight of HP-PA-NDs at temperatures greater than ~ 300°C in thermogravimetric analysis (TGA, Supplementary **Figure S1**).

To determine more precisely the loading capacity of PA-ND with HP, we followed a standard protocol based on the tolonium chloride reaction to measure the concentration of HP in DDW before and after addition of PA-ND particles into the solution. From the difference in the HP concentration, we calculated a loading capacity of 77 ± 3 mg/g and 31 ± 2 mg/g at saturation for 35-nm and 100-nm NDs, respectively. Without the PA-coating, the amount of the HP adsorbed is ~ 20-fold less. A close examination for the stability of the HP-PA-ND conjugates revealed that the noncovalent bonding between the highly negatively charged HP polymers and the polycationic PA-ND particles is so strong that no significant release (less than 10%) of HP from HP-PA-NDs occurred after 24 h incubation of the particles in phosphate-buffered saline (PBS, Supplementary **Figure S2**). It implies that the PA-coated ND can act as a slow-release carrier of HP.

As a potential anticoagulant, the HP-PA-ND was first investigated for its functionality *in vitro*. It is known that the dominant function of HP lies in the binding of its specific pentasaccharide sulfation sequence with AT-III. The sequence consists of GlcNAc(6S)-GlcA-GlcNS(3S,6S)-IdoA-GlcNS(6S), where NS, 2S, 3S and 6S represent N-, 2-O-, 3-O- and 6-O- sulfates, respectively[29]. Whether this sequence contained within the HP polymer attached to PA-NDs is available for the interaction with AT-III is a matter of concern. To address this issue, we performed matrix-assisted laser desorption/ionization time-of-flight mass spectrometry (MALDI-TOF MS) to examine the selective extraction ability of HP-PA-NDs for human AT-III (MW ~ 57 kDa) in the presence of other proteins such as bovine serum albumin (BSA)[41]. **Figure 2** presents positive ion MALDI-TOF mass spectra of the protein mixture with a weight ratio of AT-III:BSA = 1:1 before and after extraction with HP-PA-NDs using sinapinic acid as the matrix. The spectral comparison between these two sets of data clearly shows an enhancement of the AT-III peak after the extraction. The HP indeed retains its functionality after adsorption onto PA-NDs.

Hemocompatibility of oxidized HPHT-NDs. The hemolytic activity of NDs was studied following standard protocols using human RBCs as the samples[10,15,42–45]. The principle of the method is that hemolysis results in the release of hemoglobin, which is deep red-colored and can be detected by colorimetry. We employed NDs of 4 different dimensions in this study: 35, 100, 250, and 500 nm. Dose-dependent analyses were carried out in a 96-well plate with PBS as a negative control and DDW as a positive control. Apart from NDs, GOs were also used for comparison. **Figure 3a and 3b** display results of the hemolytic activity measurements, where nanoparticles of different size and types were incubated with human RBCs at room temperature for 2 h, after which they were removed by centrifugation prior to colorimetric analysis. Irrespective of the particle size, all NDs showed no sign of RBC destruction at the concentration as high as 400 µg/mL. In contrast, the membrane of the
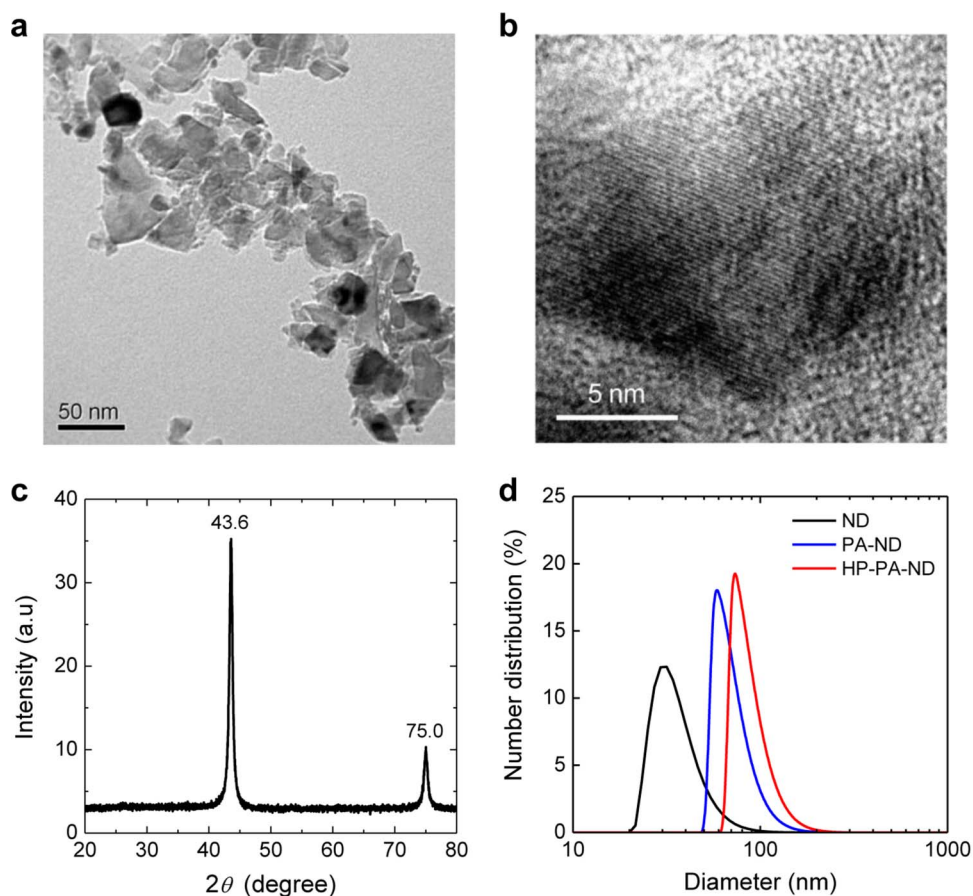
Figure 1 | **Characterization of 35-nm NDs and their bioconjugates.** (a) TEM image of the ND sample after air oxidation and strong oxidative acid treatment. (b) High-resolution TEM image of the ND particle, showing monocrystalline structure of the diamond matrix. (c) X-ray diffraction pattern of the ND powders exhibiting two distinct peaks at $2\theta = 43.6°$ and $75.0°$, corresponding to the (111) and (220) planes of crystalline diamond, respectively. (d) Size distributions of the NDs before and after surface modification with PA and subsequently with HP, measured by dynamic light scattering. The number-averaged diameters of NDs, PA-NDs, and HP-PA-NDs in water are 38 ± 4, 77 ± 2, and 91 ± 4 nm, respectively.

RBCs incubated with GOs was substantially damaged, leading to the release of free hemoglobin in the supernatant at the dose higher than 25 μg/mL. Further examination for cell morphology with optical microscopy confirmed the intactness of the RBCs incubated with NDs of all sizes in normal saline at 100 μg/mL (Supplementary **Figure S3**).

Next, we examined the thrombogenicity of the oxidized HPHT-NDs *in vitro* with the activated partial thromboplastin time (aPTT) test, a technique commonly used to evaluate the functionality of the blood clotting systems. In this experiment, NDs (or GOs) were first added to serum isolated from human blood. After incubation for 10 min, the nanoparticle-containing serum was analyzed with an aPTT kit consisting of phospholipid, a surface activator, and $CaCl_2$. In accord with previous findings by Cheng *et al.*[15], GOs exhibited a significant anticoagulant activity at 25 μg/mL (**Figure 4**), accompanied with a dramatic increase of the aPTT from 33 s (control) to $\sim$ 3000 s at the particle concentration of 400 μg/mL due to the presence of a high density of carboxyl groups on their surfaces. The oxidized NDs (35–500 nm in diameter), by contrast, were

completely inert, showing neither thrombogenic potential nor anti-coagulant activity in the same concentration range. The lack of the thrombogenic activity of NDs stands as a sharp contrast to that of CNTs[23–25] and other nanoparticles (such as mesoporous silica nano-particles[43–45]) which, depending on the precursor states, various surface modification strategies have to be applied in order to prevent thrombogenesis from occurring.

To further evaluate the hemocompatibility of the HPHT-NDs, cell viability analysis was performed by using human umbilical vein endothelial cells (HUVECs) and the CCK-8 assay. The HUVECs were isolated from human umbilical veins, thus providing a stringent test for the hemocompatibility and safety of the nanomaterials to be used in humans. **Figure 5** displays experimental data obtained for cells incubated with 35-nm NDs at the doses of $25 - 200$ μg/mL in M199 culture medium. No cytotoxicity was found even when up to 200 μg/mL of NDs and HP-PA-NDs were added to the HUVEC culture for 18 h. Independent tests with the MTS assay also yielded similar results (Supplementary **Figure S4**). GOs, by contrast, showed a significant toxicity at the concentration as low as 50 μg/mL, a result in agreement with previous reports using different assays and cell types[10,17]. The analysis, together with the hemocompatibility assays carried out above, demonstrates that the cytotoxicity of oxidized HPHT-NDs is exceptionally low and establishes the suitability of HP-PA-NDs for biomedical applications as described below.

Anticoagulation ability of HP-conjugated NDs. HP is a widely used injectable anticoagulant in medicine. MALDI-MS analysis in

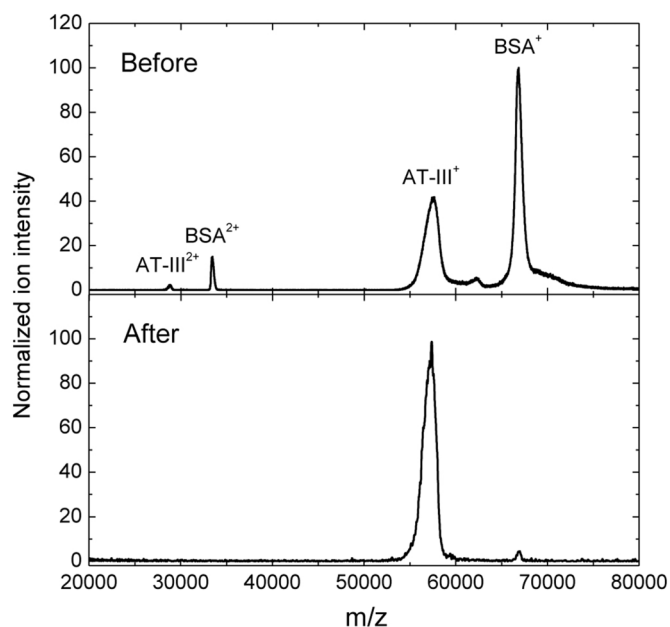| Table 1	Hydrodynamic sizes and zeta potentials of NDs, PA-NDs, and HP-PA-NDs suspended in water	
Material	Hydrodynamic size (nm)	Zeta potential (mV)
ND	38 ± 4	-34 ± 3
PA-ND	77 ± 2	$+52 \pm 2$
HP-PA-ND	91 ± 4	-43 ± 4

Figure 2 | Positive ion MALDI-TOF mass spectra of a protein mixture before and after extraction with HP-PA-NDs. The mixture consisted of AT-III and BSA with a weight ratio of 1 : 1.

Figure 2 has shown that the biopolymer retains its functionality to interact with AT-III even after adsorption onto PA-NDs prepared with 35-nm NDs. To further elucidate this effect, experiments concerning the anticoagulation ability of the HP-PA-NDs in blood were performed *ex vivo*. We first suspended HP-PA-NDs in normal saline and then injected them into the tail veins of adult mice (weighing 20–25 g each) at a dose of ∼ 50 μg per treatment. About 10 min after the injection, whole blood of the mice was collected for serum separation and aPTT tests. **Figure 6a** presents the results for i.v.-injected NDs, PA-NDs, and HP-PA-NDs. In accord with the *in vitro* studies using human blood (**Figure 4**), no

evidence of ND-induced blood coagulation was found *ex vivo* for mice treated with bare NDs. With the aid of the HP coating, however, the nanoparticles significantly prolonged the clot formation time from 43 s to 58 s. Although the lengthening of this time is significantly less than that (43 s → 70 s) of free HP injected at the dose of 20 U/kg body weight (1U ≡ 4.8 μg), which served as a positive control, the result supports the suggestion that HP-PA-ND is useful as a nanoparticle-based anticoagulant.

For the administration of free HP *in vivo*, previous pharmacokinetics studies of HP elimination in rats have shown a dose-dependent behavior[46]. The average half-life of the HP elimination is ∼ 30 min at the dose of 20 U/kg. Hence, constant-rate i.v. infusion of the anticoagulant is required in order to prevent clot formation over an extended period of time[47]. Compared with free HP, HP-PA-NDs hold the advantage of having a longer circulation half-life, which can be as long as 5 h, as reported for HP-bearing polymeric nanoparticles in blood[48]. They are potentially useful for prolonged anticoagulation applications. To demonstrate the feasibility of this approach, we applied HP-PA-NDs to a mouse model with hindlimb thromboembolism[34]. In this experiment, arteries and veins of the hindlimbs of adult mice were exposed by surgery and then treated with 5% FeCl$_3$ in a H$_2$O-saturated patch for 3 min to induce blood clotting. Afterwards, normal saline (negative control), HP (positive control), NDs, or HP-PA-NDs were introduced into the mice by i.v. injection. Hindlimb blood flow rates were then measured at different time points by laser Doppler flowmetry. As the time required to obtaining reliable data after the i.v. injection was ∼ 15 min, we present only data collected after this time period in **Figure 6b**. Results show that the HP-PA-ND particles have a significantly higher antithrombotic activity than free HP, whose effect disappeared almost completely within 15 min post-injection[34]. Note that this half-life is considerably shorter than that of free HP in uninjured rats[46]. The nanoparticle-based treatment, indeed, is able to extend the thrombus formation time far longer (>40 min) than that of the injection of free HP alone.

Finally, the hypothesis that the presence of oxidized and HP-conjugated NDs in blood will not activate the acute systemic inflammatory response was tested with the inflammatory cytokine analysis
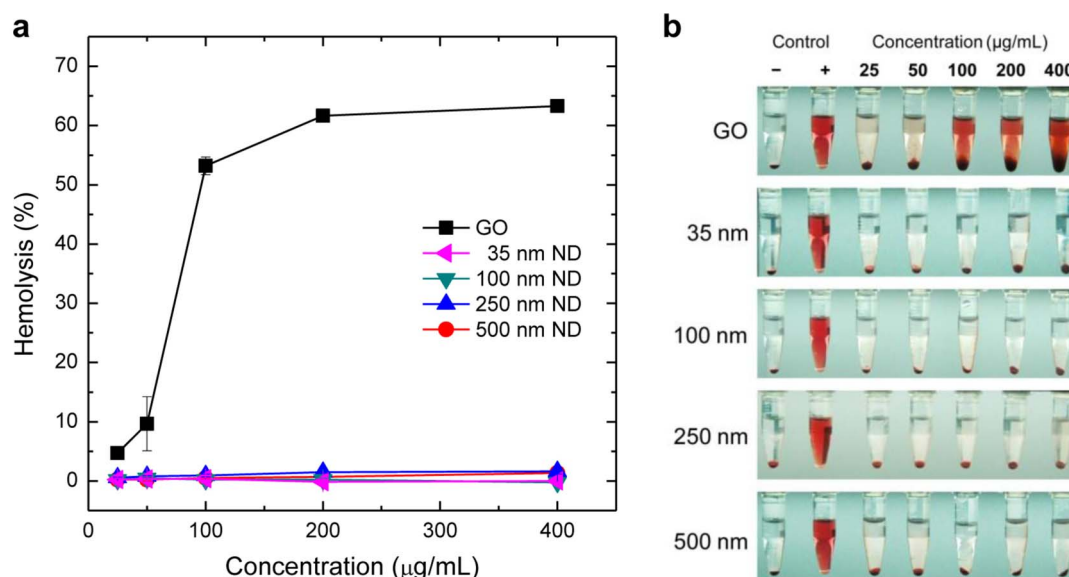

Figure 3 | Hemolysis studies of GOs and oxidized NDs of different size with human RBCs. (a) Hemolysis percentages measured at the concentration range of 25–400 μg/mL for GOs and 4 different ND samples (35, 100, 250, and 500 nm in diameter) incubated with RBCs at 25°C for 2 h. GOs served as the positive control. (b) Photographs of human RBCs treated with GOs and NDs of 4 different size at the concentration range of 25–400 μg/mL. The red color of the solution is due to the release of hemoglobin from the damaged RBCs, and the red pellets at the bottom of the Eppendorf tubes are intact RBCs precipitated by centrifugation. PBS and DDW served as the negative (−) and positive (+) controls, respectively. The experiments were repeated in triplicate.
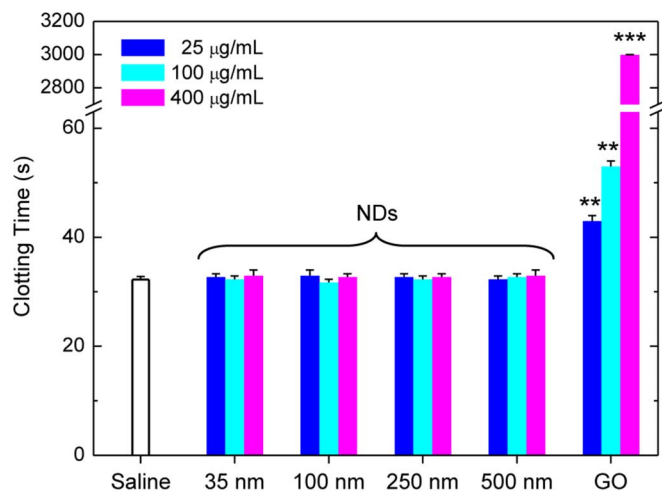
4

Figure 4 | Activated partial thromboplastin time (aPTT) assays of GOs and oxidized NDs of different size using human serum. Compared to NDs and normal saline, which served as the negative control, GOs clearly showed an anticoagulant activity ($**p < 0.01$ and $***p < 0.001$). The experiments were repeated in triplicate.

Figure 5 | Cell viability tests of HUVECs treated with NDs, HP-PA-NDs, and GOs. The tests were carried out by using the CCK-8 assay. No cytotoxic effects were observed for cells treated with NDs and HP-PA-NDs at the concentration range of 25–200 μg/mL for 18 h, whereas a dose-dependent toxicity was detected for GOs under the same experimental conditions. The experiments were repeated in triplicate.

using the mouse model. In this experiment, blood was collected from adult mice at 6 h after i.v. injection of 35-nm NDs and their variants through tail veins at the dose of 50 mg/kg. Serum separated from the blood was then analyzed for the inflammation-related cytokines (e.g. IL-1β and IL-6) using the standard mouse ELISA kits. With lipopolysaccharide (LPS), which is known to induce a strong response from animal immune systems[49], as the positive control, we found no significant increase in the level of these two cytokines for both the ND and HP-PA-ND treatments (**Figure 7**). Moreover, no mice died during the course of the measurements even though they had been treated with such a high dose (~1 mg per mouse) of NDs. The results are in line with the findings of the aforementioned hemolysis and thrombogenicity assays (**Figures 3** and **4**).

Discussion

In recent years, a rich variety of nanomaterials have been proposed for gene and drug delivery *in vivo* through i.v. administration. However, the biocompatibility and hemocompatibility of these nanomaterials are of the major concerns. As a member in the list of the nanocarbon family, nanoscale diamond holds great promise and potential for the applications and how it interacts with blood components deserves close examination. In this work, we have performed a systematic investigation using various assays (both *in vitro* and *in vivo*) and found that HPHT-synthesized monocrystalline NDs after air oxidation and strong oxidative acid treatment have excellent hemocompatibility with negligible hemolytic and thrombogenic activities. The hemocompatibility is distinctly better than that of graphene oxides intended for biomedical applications. We attribute this unique property to the low aspect ratio of the nanomaterial as well as the high affinity of the oxidized HPHT-NDs for proteins. We have previously reported that HPHT-NDs after extensive treatment with oxidative acids bind strongly with proteins of various types and sizes in PBS[50]. Blood protein components such as serum albumin can be captured in seconds by the acid-treated NDs upon mixing[50,51]. Such a high affinity is established through the interplay of electrostatic force, hydrogen bonding, and hydrophobic interactions between surface and adsorbate. It is the so-called protein corona effect[9] that effectively prevents both erythrocyte membrane damage and blood clotting from occurring.

Another benefit of the protein corona effect is that it helps reduce agglomeration of NDs in PBS or other biological buffers. Agglomeration of nanoparticles in physiological environments is a general
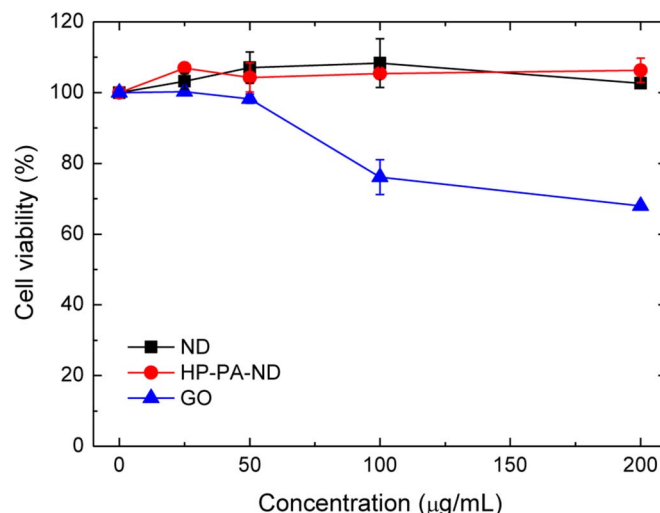
phenomenon and has been observed for nanomaterials of various types. It has raised concerns about the efficacy of using nanoparticles as drug delivery vehicles. A number of strategies, including noncovalent coating with amphiphilic triblock copolymers, BSA, etc.[52], have been developed recently and applied to stabilize inorganic particles such as magnetic beads and gold nanoparticles in high ionic strength media. We have previously found that BSA is an excellent stabilizing agent for NDs[53]. The BSA-coated NDs can resist flocculation for more than 5 days in PBS. For HPHT-NDs noncovalently coated with human serum albumin (HSA), they show similarly high stability and dispersibility in PBS (Supplementary **Figure S5**) and thus are useful for drug delivery applications. These particles are preferentially accumulated in livers and spleens after i.v. injection into mice, as have been reported by Yuan *et al.*[54] for BSA-coated NDs.

This work demonstrates that monocrystalline NDs after proper surface modification with polyarginine can act as a novel drug carrier for heparin, the most widely used anticoagulant for treating thromboembolism. The anticoagulant action of the HP-PA-NDs is made possible by escape of the nanoparticle bioconjugates from opsonization. Although the HP adsorbed on PA-ND has a lower anticoagulant activity than its free HP counterpart (**Figure 6a**), the advantage of using HP-PA-ND as an anticoagulant is apparent when prolonged anticoagulation treatment is in need (**Figure 6b**). The reasons why the adsorbed HP is less active than free HP include that (i) some active sites of the HP are blocked after adsorption onto PA-ND and (ii) some HP-PA-ND particles form aggregates in blood after administration.

Lastly, our results show that the i.v. injection of either bare or HP-PA-conjugated NDs into adult mice will not cause any significant increase in the cytokine levels of IL-1β and IL-6 in their bloodstream. The absence of the ND-induced inflammation is also likely to be a consequence of the protein corona effect, with which the activation of the immune system by the foreign substances is avoided. Having perfect hemocompatibility and exceptionally low cytotoxicity, the sp^3-carbon-based nanoparticles are expected to find wide applications as drug delivery devices for the treatment of blood-related diseases and other health issues as well. The present study paves the way for future therapeutic applications of NDs in biology and medicine.
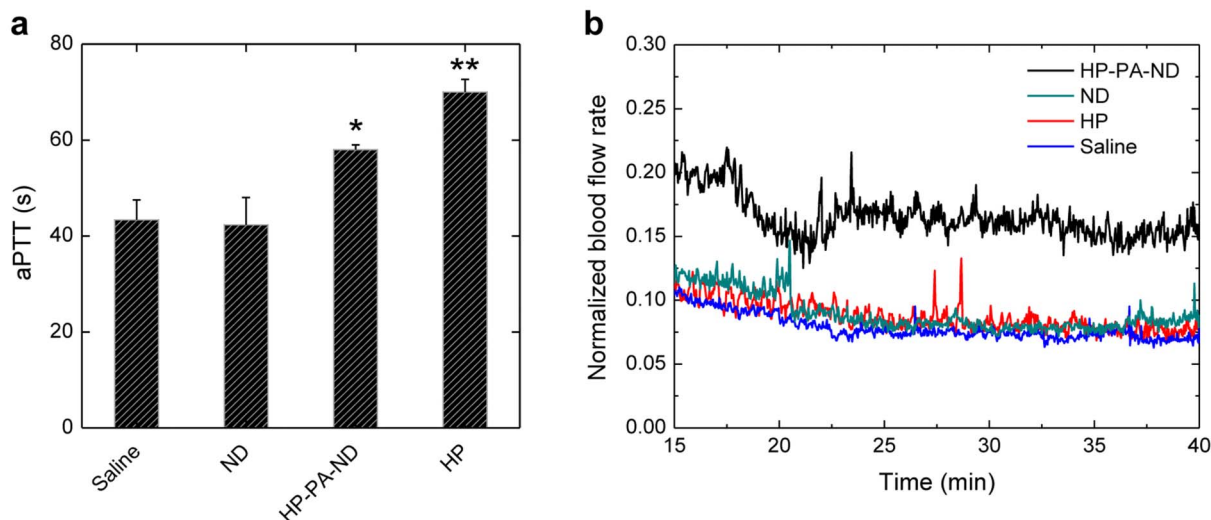
Figure 6 | Comparison of the anticoagulant activities of HP and HP-PA-NDs both *ex vivo* and *in vivo*. (a) *Ex vivo* analysis with aPTT tests for serum extracted from mice treated with normal saline, NDs (2 mg/kg), HP (20 U/kg), and HP-PA-NDs (2 mg/kg) via i.v. injection. Compared to normal saline and ND, HP and HP-PA-ND clearly showed anticoagulant activities (*$p < 0.05$ and **$p < 0.01$). The experiments were repeated in triplicate. (b) *In vivo* analysis for the prevention of thrombus formation with HP and HP-PA-ND in a mouse model of acute thromboembolism. The analysis was made after i.v. injection of normal saline, NDs (2 mg/kg), HP (20 U/kg), and HP-PA-NDs (2 mg/kg) into hindlimb-ischemia mice with thrombosis induced by $FeCl_3$. At 15 min post-injection, the free HP exhibited almost no anticoagulant activity, as measured by laser Doppler flowmetry. In contrast, the HP-PA-NDs prolonged the blood flow and effectively prevented the thrombus formation up to 40 min post-injection. All the blood flow data were normalized against the corresponding reference flow rates measured for the other hindlimbs of the same mice without surgery and treatments.

Methods

Materials. Synthetic HPHT diamond powders of four different sizes were obtained from Microdiamant (MSY 0–0.05) and Element Six (Micron + MDA M0.10, M0.25, M0.5), respectively. GOs were synthesized with graphite powders following procedures previously described[55].

Material characterization. NDs were imaged with a transmission electron microscope (H-7100, Hitachi) after applying the particles onto a copper grid surface. Powder X-ray diffraction patterns of NDs were obtained by using an X-ray diffractometer (XRD-7000, Shimadzu) with Cu-Kα radiation. Size distributions and surface charge states of the ND particles in DDW were determined by using a particle size and zeta-potential analyzer (Delsa Nano C, Beckman-Coulter).

Surface modification. Raw ND materials of different size were oxidized in air at 450°C for 1 h and then treated in concentrated H_2SO_4-HNO_3 (3 : 1, v/v) solution at 100°C in a microwave reactor (Discover BenchMate, CEM) for 3 h to form carboxylated/oxidized surfaces. Coating of the carboxylated/oxidized NDs with PA (MW 15–70 kDa, Sigma-Aldrich) was conducted via EDC/NHS-mediated coupling reactions as detailed in refs. 38 and 39. Briefly, EDC, NHS, and acid-treated NDs with the weight ratio of 1 : 1 : 1 were mixed together in 0.1 M MES buffer (Sigma-Aldrich) at pH 6. After incubation for 15 min, the NHS-activated NDs were thoroughly washed by PBS (pH 7.4, Gibco) to remove excess EDC and NHS, and then mixed with PA in PBS by gentle shaking at room temperature for 2 h. The PA-conjugated ND particles were finally collected by centrifugation, thoroughly washed with DDW, and prepared as a suspension after the last wash.

HP adsorption capacity and release profile. HP (H5515, Sigma-Aldrich) was dissolved in DDW and then mixed with the PA-ND suspension of known concentration by gentle shaking for 30 min, after which the mixture was centrifuged and the supernatant was collected. Concentrations of HP in the supernatant were determined by adding 5% toluidine blue O (Sigma-Aldrich) to the solution at a v/v ratio of 1 : 4 for 3 min, followed by mixing with hexane at a v/v ratio of 1 : 1 for 3 min. A UV-visible spectrophotometer (U-3310, Hitachi) measured the absorbance of the mixture at 631 nm. The same assay was applied to determine the HP release profile of HP-PA-NDs dispersed in PBS.

Selective protein extraction and MALDI-TOF MS. Proteins were mixed with saturated sinapinic acid (Sigma-Aldrich) dissolved in acetonitrile/H_2O solution (v/v = 2 : 1) containing 0.1% trifluoroacetic acid for MALDI plate spotting. Positive ion MS spectra were acquired with a reflection TOF mass spectrometer (Microflex, Bruker-Daltonics). To investigate the selective extraction ability of HP-PA-NDs, AT-III (Sigma-Aldrich) and BSA (Sigma-Aldrich) were mixed with the particles at the weight ratios of 1 : 1 : 40 in PBS. After mixing for 15 min, unbound proteins were removed by extensive washes of the nanoparticles with 20 mM Tris (pH 8) and the protein-loaded HP-PA-NDs were collected as pellets by centrifugation. MALDI matrix solution was then added to the pellets to elute the adsorbed proteins from the nanoparticles to form a slurry. About 1 μL of the slurry was deposited on the MALDI probe for TOF-MS analysis.

Hemolysis assay. Fresh human whole blood from a volunteer donor was stabilized with ethylenediamine tetraacetic acid (EDTA). Serum was removed from the blood sample by centrifugation at 200 *g* for 5 min. Remaining RBCs were washed five times with sterile isotonic PBS and then diluted 10 × with the same solution after the last wash. To determine the hemolytic activity of NDs (or GOs), diluted RBC suspension (0.2 mL, ~ 4 × 10⁸ cells/mL) was added to the nanoparticle suspension (0.8 mL) prepared with PBS at different concentrations (25–400 μg/mL). After vortexing the
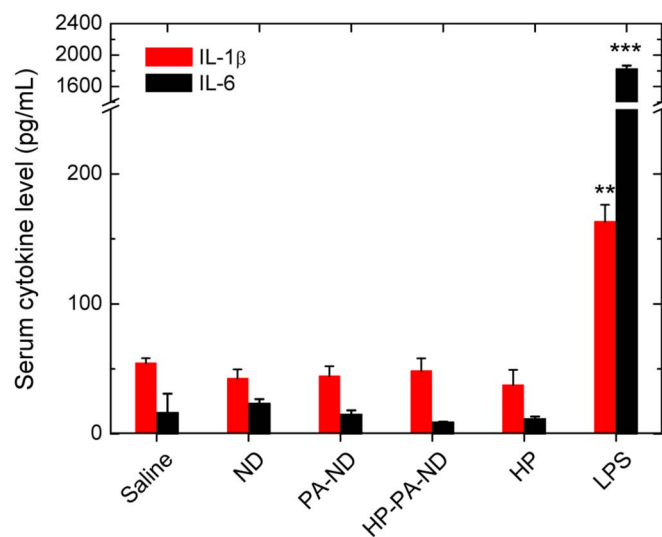

Figure 7 | Measurements of the systemic inflammatory cytokine levels of serum IL-1β and IL-6 following i.v. injection of oxidized and HP-conjugated NDs into mice. Normal saline and LPS (lipopolysaccharide) served as the negative and positive controls, respectively. The levels measured for both cytokines showed no significant inflammation induced by the ND, PA-ND, and HP-PA-ND particles at the dose of 50 mg/kg, in marked difference to the LPS treatment (**$p < 0.01$ and ***$p < 0.001$). The experiments were repeated in triplicate.

mixtures at room temperature for 2 h, NDs (or GOs) and intact RBCs were removed by centrifugation. A microplate reader (Thermo Scientific) measured the absorbance (A) of the hemoglobin in the supernatant at 570 nm, with the absorbance at 620 nm as a reference, and the hemolysis percentage was calculated as

$$\% \text{ hemolysis} = \frac{\text{Sample A}_{570-620} - \text{Negative control A}_{570-620}}{\text{Positive control A}_{570-620} - \text{Negative control A}_{570-620}} \times 100$$

In vitro aPTT test. Serum was separated from human blood in sodium citrate by centrifugation at 2500 g and 4°C for 20 min. It was then mixed with the ND (or GO) suspension of known concentration (25–400 µg/mL) and the aPTT test solution (CEPHEN 5, Aniara) at the volume ratio of 9 : 1 : 10. After incubation at 37°C for 3 min, the sample solution was added with 25 mM CaCl$_2$ (0.1 mL) and the time of clot formation was recorded.

Cell viability assay. HUVECs (PCS-100-01, ATCC) were maintained in M199 culture medium supplemented with endothelial growth medium (EGM), 20% fetal bovine serum (Biological Industries), and 1% penicillin-streptomycin (5000 U/mL, Gibco) at 37°C with 5% CO$_2$. Cell viability assays were carried out by first seeding the cells in primary cell culture medium at a density of 5×10^4 cells/well in a 96-well plate, followed by incubation at 37°C with 5% CO$_2$ overnight for cell attachment. Cells were then incubated with 25–200 µg/mL NDs, HP-PA-NDs, or GOs for 18 h, after which free nanoparticles were removed by thorough washing of the cells with serum-free M199 medium. Fresh maintenance medium and the CCK-8 solution (Cell Counting Kit-8, Sigma-Aldrich) were then added to the cultures for cell viability analysis. The assays were performed according to the manufacturer's instructions with the absorbance of the reaction products measured at 450 nm.

Animals. FVB mice were acclimated for 8–12 weeks in the animal facilities of National Cheng Kung University. The animals were maintained under specific pathogen-free conditions and were treated benevolently to eliminate or reduce suffering during the entire study. Experiments were conducted with compliance of standards established in the Guide for the Care and Use of Laboratory Animals, with procedures approved by the Institutional Animal Care and Use Committee of National Cheng Kung University[34].

Ex vivo aPTT test. ND particles suspended in normal saline (0.5 mg/mL) were injected intravenously at a dose of 2 mg/kg into the tail veins of adult mice. After 10 min, whole blood was collected for serum separation and aPTT tests. The positive control consisted of HP injected at a dose of 20 U/kg (1U ≡ 4.8 µg) and normal saline served as the negative control.

Thromboembolism model. FVB mice (8–12 weeks old and weighing 20–25 g) were used for the hindlimb thromboembolism model, as previously described[34]. Briefly, mice were first anesthetized with Zoteil-50 (50 mg/kg, i.p., Vibrac). The femoral artery and vein of the hindlimb of each mouse were then exposed by piercing through the membranous femoral sheath, and separated from the nerve for exposure to 5% FeCl$_3$ (Sigma-Aldrich) in a DDW-saturated patch. After 3 min of the exposure, the patch was removed, and the incision was sutured with 6-0 sutures. Hindlimb blood flow rates were measured by using a laser Doppler flowmeter (O2C, LEA Medizintechnik). To treat the FeCl$_3$-induced acute thromboembolism, ND particles suspended in normal saline (0.5 mg/mL) were injected intravenously at a dose of 2 mg/kg into the tail veins of the hindlimb-ischemia mice. Pure HP injected at a dose of 20 U/kg served as the positive control and normal saline was used as the negative control. All the blood flow data were normalized against the corresponding reference flow rates measured for the other hindlimbs of the same mice without surgery and treatments.

Inflammatory cytokine assay. Blood was collected from mice at 6 h after i.v. injection of NDs or their variants suspended in normal saline (10 mg/mL) at a dose of 50 mg/kg through tail veins. Samples were centrifuged at 1500 g for 10 min to obtain serum, which was then analyzed using the ELISA kits (AssayPro) for the detection of mouse IL-1β and IL-6 cytokines, following the manufacturer's instructions. The positive control consisted of LPS injected at a dose of 5 mg/kg and normal saline served as the negative control.

Statistical analysis. All data were presented as mean ± standard deviation. Statistical analysis was performed using two tailed t-tests and only p-values of the samples that showed significant differences were reported.

1. Bianco, A., Kostarelos, K. & Prato, M. Opportunities and challenges of carbon-based nanomaterials for cancer therapy. *Expert Opin. Drug Deliv.* **5**, 331–342 (2008).
2. Cha, C., Shin, S. R., Annabi, N., Dokmeci, M. R. & Khademhosseini, A. Carbon-based nanomaterials: Multifunctional materials for biomedical engineering. *ACS Nano* **7**, 2891–2897 (2013).
3. Fiorito, S., Serafino, A., Andreola, F., Togna, A. & Togna, G. Toxicity and biocompatibility of carbon nanoparticles. *J. Nanosci. Nanotechnol.* **6**, 591–599 (2006).
4. Schrand, A. M. et al. [Cytotoxicity and genotoxicity of carbon nanomaterials] *Safety of Nanoparticles, Nanostructure Science and Technology* [Webster, T. J. (ed.)] 159–187 (Springer: New York, 2009).
5. Kolosnjaj, J., Szwarc, H. & Moussa, F. Toxicity studies of carbon nanotubes. *Adv. Exp. Med. Biol.* **620**, 181–204 (2007).
6. Fisher, C. et al. Applications and nanotoxicity of carbon nanotubes and graphene in biomedicine. *J. Nanomater.* **2012**, 315185 (2012).
7. Feng, L. & Liu, Z. Graphene in biomedicine: Opportunities and challenges. *Nanomedicine* **6**, 317–324 (2011).
8. Wang, K. et al. Biocompatibility of graphene oxide. *Nanoscale Res. Lett.* **6**, 8 (2011).
9. Hu, W. et al. Protein corona-mediated mitigation of cytotoxicity of graphene oxide. *ACS Nano* **5**, 3693–3700 (2011).
10. Liao, K.-H., Lin, Y.-S., Macosko, C. W. & Haynes, C. L. Cytotoxicity of graphene oxide and graphene in human erythrocytes and skin fibroblasts. *ACS Appl. Mater. Interfaces* **3**, 2607–2615 (2011).
11. Singh, S. K. et al. Thrombus inducing property of atomically thin graphene oxide sheets. *ACS Nano* **5**, 4987–4996 (2011).
12. Sasidharan, A. et al. Hemocompatibility and macrophage response of pristine and functionalized graphene. *Small* **8**, 1251–1263 (2012).
13. Chen, G.-Y. et al. Simultaneous induction of autophagy and toll-like receptor signaling pathways by graphene oxide. *Biomaterials* **33**, 6559–6569 (2012).
14. Yue, H. et al. The role of the lateral dimension of graphene oxide in the regulation of cellular responses. *Biomaterials* **33**, 4013–4021 (2012).
15. Cheng, C. et al. Biopolymer functionalized reduced graphene oxide with enhanced biocompatibility via mussel inspired coatings/anchors. *J. Mater. Chem. B* **1**, 265–275 (2013).
16. Schranda, A. M., Dai, L., Schlager, J. J., Hussain, S. M. & Osawa, E. Differential biocompatibility of carbon nanotubes and nanodiamonds. *Diam. Relat. Mater.* **16**, 2118–2123 (2007).
17. Zhang, X., Hu, W., Li, J., Tao, L. & Wei, Y. A comparative study of cellular uptake and cytotoxicity of multi-walled carbon nanotubes, graphene oxide, and nanodiamond. *Toxicol. Res.* **1**, 62–68 (2012).
18. Mochalin, V. N., Shenderova, O., Ho, D. & Gogotsi, Y. The properties and applications of nanodiamonds. *Nat. Nanotechnol.* **7**, 11–23 (2012).
19. Evani, S. J. & Ramasubramanian, A. K. Hemocompatibility of nanoparticles, in *Nanobiomaterials Handbook* Sitharaman, B. (ed.) CRC Press, 2011, Chap. 31.
20. Liu, K.-K. et al. Covalent linkage of nanodiamond-paclitaxel for drug delivery and cancer therapy. *Nanotechnology* **21**, 315106 (2010).
21. Chow, E. K. et al. Nanodiamond therapeutic delivery agents mediate enhanced chemoresistant tumor treatment. *Sci. Transl. Med.* **3**, 73ra21 (2011).
22. Trpkovic, A. et al. Oxidative stress-mediated hemolytic activity of solvent exchange-prepared fullerene (C$_{60}$) nanoparticles. *Nanotechnology* **21**, 375102 (2010).
23. Radomski, A. et al. Nanoparticle-induced platelet aggregation and vascular thrombosis. *Brit. J. Pharmacol.* **146**, 882–893 (2005).
24. Burke, A. R. et al. Determinants of the thrombogenic potential of multiwalled carbon nanotubes. *Biomaterials* **32**, 5970–5978 (2011).
25. Lacerda, S. H. et al. Carbon nanotubes activate store-operated calcium entry in human blood platelets. *ACS Nano* **5**, 5808–5813 (2011).
26. Puzyr, A. P. et al. Destruction of human blood cells in interaction with detonation nanodiamonds in experiments in vitro. *Diam. Relat. Mater.* **13**, 2020–2023 (2004).
27. Kumari, S., Singh, M. K., Singh, S. K., Grácio, J. J. & Dash, D. Nanodiamonds activate blood platelets and induce thromboembolism. *Nanomedicine* DOI:10.2217/NNM.13.23 (2013).
28. Lin, Y.-C. et al. The influence of nanodiamond on the oxygenation states and micro-rheological properties of human red blood cells in vitro. *J. Biomed. Opt.* **17**, 101512 (2012).
29. Björk, I. & Lindahl, U. Mechanism of the anticoagulant action of heparin. *Mol. Cell. Biochem.* **48**, 161–182 (1982).
30. Chong, B. H. Heparin-induced thrombocytopenia. *J. Thromb. Haemost.* **1**, 1471–1478 (2003).
31. Gutowska, A., Bae, Y. H., Feijen, J. & Kim, S. W. Heparin release from thermosensitive hydrogels. *J. Control. Release* **22**, 95–104 (1992).
32. Ahola, M. S. et al. In vitro release of heparin from silica xerogels. *Biomaterials* **22**, 2163–2170 (2001).
33. Park, T.-J. et al. Preparation and characterization of heparinized multi-walled carbon nanotubes. *Process Biochem.* **47**, 113–118 (2012).
34. Tang, A. C. L. et al. Treatment of acute thromboembolism in mice using heparin-conjugated carbon nanocapsules. *ACS Nano* **6**, 6099–6107 (2012).
35. Tang, A. C. et al. Biosafety of non-surface modified carbon nanocapsules as a potential alternative to carbon nanotubes for drug delivery purposes. *PLoS One* **7**, e33893 (2012).
36. Huang, L. C. L. & Chang, H.-C. Adsorption and immobilization of cytochrome c on nanodiamonds. *Langmuir* **20**, 5879–5884 (2004).
37. Nguyen, T. T.-B., Chang, H.-C. & Wu, V. W.-K. Adsorption and hydrolytic activity of lysozyme on diamond nanocrystallites. *Diamond Relat. Mater.* **16**, 872–876 (2007).
38. Chang, C.-K., Wu, C.-C., Wang, Y.-S. & Chang, H.-C. Selective extraction and enrichment of multi-phosphorylated peptides using polyarginine-coated diamond nanoparticles. *Anal. Chem.* **80**, 3791–3797 (2008).

39. Hsieh, C.-C. *et al.* Quantitative analysis of oligosaccharides derived from sulfated glycosaminoglycans by nanodiamond-based affinity purification and MALDI MS. *Anal. Chem.* **85**, 4342–4349 (2013).
40. Vial, S. *et al.* Peptide-grafted nanodiamonds: Preparation, cytotoxicity and uptake in cells. *Chembiochem.* **9**, 2113–2119 (2008).
41. Belgacem, O. *et al.* Molecular mass determination of plasma-derived glycoproteins by ultraviolet matrix-assisted laser desorption/ionization time-of-flight mass spectrometry with internal calibration. *J. Mass Spectrom.* **37**, 1118–1130 (2002).
42. Dobrovolskaia, M. A. *et al.* Method for analysis of nanoparticle hemolytic properties *in vitro*. *Nano Lett.* **8**, 2180–2187 (2008).
43. Slowing, I. I., Wu, C.-W., Vivero-Escoto, J. L. & Lin, V. S. Mesoporous silica nanoparticles for reducing hemolytic activity towards mammalian red blood cells. *Small* **5**, 57−62 (2009).
44. Lin, Y.-S. & Haynes, C. L. Impacts of mesoporous silica nanoparticle size, pore ordering, and pore integrity on hemolytic activity. *J. Am. Chem. Soc.* **132**, 4834−4842 (2010).
45. Yildirim, A., Ozgur, E. & Bayindir, M. Impact of mesoporous silica nanoparticle surface functionality on hemolytic activity, thrombogenicity and non-specific protein adsorption. *J. Mater. Chem. B* **1**, 1909–1920 (2013).
46. Bjornsson, T. D. & Gerhard, L. Pharmacokinetics of heparin. I. Studies of dose dependence in rats. *J. Pharmacol. Exp. Ther.* **210**, 237–242 (1979).
47. Bjornsson, T. D. & Gerhard, L. Pharmacokinetics of heparin. II. Studies of time dependence in rats. *J. Pharmacol. Exp. Ther.* **210**, 243–246 (1979).
48. Passirani, C., Barratt, G., Devissaguet, J.-P. & Labarre, D. Long-circulating nanoparticles bearing heparin or dextran covalently bound to poly(methyl methacrylate). *Pharm. Res.* **15**, 1046–1050 (1998).
49. Raetz, C. & Whitfield, C. Lipopolysaccharide endotoxins. *Annu. Rev. Biochem.* **71**, 635−700 (2002).
50. Kong, X. L. *et al.* High-affinity capture of proteins by diamond nanoparticles for mass spectrometric analysis. *Anal. Chem.* **77**, 259–265 (2005).
51. Chen, W.-H. *et al.* Solid phase extraction and elution on diamond (SPEED): A fast and general platform for proteome analysis with mass spectrometry. *Anal. Chem.* **78**, 4228–4234 (2006).
52. Lim, J. K., Majetich, S. A. & Tilton, R. D. Stabilization of superparamagnetic iron oxide core – gold shell nanoparticles in high ionic strength media. *Langmuir* **25**, 13384–13393 (2009).
53. Tzeng, Y.-K. *et al.* Superresolution imaging of albumin-conjugated fluorescent nanodiamonds in cells by stimulated emission depletion. *Angew. Chem. Int. Ed.* **50**, 2262–2265 (2011).
54. Yuan, Y., Chen, Y., Liu, J. H., Wang, H. & Liu, Y. Biodistribution and fate of nanodiamonds *in vivo*. *Diam. Relat. Mater.* **18**, 95–100 (2009).
55. Wang, D.-Y. *et al.* Quantum dot light-emitting diode using solution-processable graphene oxide as the anode interfacial layer. *J. Phys. Chem. C* **116**, 10181–10185 (2012).

Acknowledgements

Author contributions

H.-C.L., F.-J.H., C.-P.C., M.-Y.C. and S.-U.H. conducted experiments, P.C.H.H., C.-C.C., C.-C.W. and H.-C.C. supplied materials and equipments, H.-C.L., F.-J.H., C.-C.W. and H.-C.C. designed experiments and wrote the manuscript.

Additional information

Supplementary information accompanies this paper at http://www.nature.com/scientificreports

Competing financial interests: The authors declare no competing financial interests.

How to cite this article: Li, H.-C. *et al.* The hemocompatibility of oxidized diamond nanocrystals for biomedical applications. *Sci. Rep.* **3**, 3044; DOI:10.1038/srep03044 (2013).